A Joint Crest Factor Reduction and Digital Predistortion for Power Amplifiers Linearization Based on Clipping-and-Bank-Filtering

Siqi Wang, Morgan Roger, Caroline Lelandais-Perrault, Julien Sarrazin

A Joint Crest Factor Reduction and Digital Predistortion for Power Amplifiers Linearization Based on Clipping-and-Bank-Filtering

Siqi Wang, Morgan Roger, *Member, IEEE*, Caroline Lelandais-Perrault, Julien Sarrazin, *Member, IEEE*

***Abstract*—A power amplifier (PA) operating point determines both its power efficiency and its linearity. A high operating point generally corresponds to a better efficiency but a poor linearity. The combination of Digital predistortion (DPD) and Crest factor reduction (CFR) enables the control of the PA operating point and the optimization of the trade-off between power efficiency and linearity. This paper proposes a novel technique for joint CFR/DPD adapted to single-carrier as well as multi-carrier signals. Compared to similar low-complexity approaches to PA linearization and efficiency enhancement, it provides better linearization performance especially when the PA operating point is chosen to be high. The CFR and DPD are here implemented as a single model so that the running complexity of the CFR is almost negligible. The CFR model coefficients are estimated through a new clipping-and-bank-filtering (CABF) method extended to multi-carrier signals. The approach is complete with a discussion on the choice of windows in the filter bank and the presentation of a multiple-step procedure to determine the best model structure. The proposed CABF-based joint CFR/DPD model is experimentally evaluated on test bench with a PA using single-carrier and 2-carrier 20 MHz long term evolution (LTE) signals as the stimulus.**

***Index Terms*—Crest factor reduction, digital predistortion, nonlinear distortion, power amplifiers**

I. Introduction

IN MODERN wireless telecommunication systems, power amplifiers (PA) consume the majority of power. Improving their power efficiency in transmitting data is an important concern for green communications [1]. The power efficiency of the PA is strongly correlated to its operating point [2]. When the PA is working near the saturation zone, the power efficiency approaches the maximum but the PA is very nonlinear.

Digital predistortion (DPD) is an efficient choice to compensate for the nonlinearities and the memory effects of the PA. Basically the DPD has the inverse characteristics of the PA and is applied upstream of the PA in a transmitter circuit [3]. Numerous DPD models based on Volterra Series have been studied, such as memory polynomial (MP) [4] [5], generalized memory polynomial (GMP) [6], dynamic-deviation-reduction (DDR) [7], complexity-reduced Volterra series (CRV) [8], and the decomposed vector rotation-based behavioral model (DVR) [9]. Block-oriented non linear (BONL) systems have also been studied as DPD [10] [11] [12].

With the linearization by DPD, the main constraint on the PA operating point is the peak-to-average power ratio (PAPR) of the modulated signal, e.g. Orthogonal Frequency Division Multiplexing (OFDM) signals [13]. In order to avoid the saturation zone, an output back-off (OBO) at least equal to the PAPR is needed.

Numerous crest factor reduction (CFR) techniques have been studied to reduce PAPR when DPD is used [14] [15] [16]. Though CFR helps increasing the PA efficiency, it deteriorates the system linearity, especially if basic hard clipping (HC) is used. The error vector magnitude (EVM) and the adjacent channel power ratio (ACPR) are often used to characterize the in-band and out-of-band errors respectively. When the ACPR requirements are more strict than that of EVM, the clip-and-filter (CAF) approach enables to trade off in-band errors for reduced out-of-band errors compared to HC [17]. CFR is usually implemented as a correction to reduce signal peaks. It can be applied at the DPD input or the DPD output —even both— with different methods [18].

Furthermore, similarly to DPD, it can be implemented as a parametric model, which we refer to as modeled CFR (MCFR). For instance, a polynomial soft clipping method has been proposed in [19] as CFR at the DPD input. The polynomial coefficients are estimated by minimizing the PAPR under the constraints of ACPR requirements. Because the soft clipping compresses only the signal amplitude, the EVM value can be improved at the receiver using a post-compensation method.

In [18], we compared traditional HC, CAF and MCFR by studying their impact on linearity for several OBO values, in the presence of DPD. Considering the computational burden added by the CFR, the MCFR applied on the DPD output signal has a great advantage. If the MCFR and the DPD share the same model structure they can be merged into a single joint CFR/DPD model whose coefficients equal the difference of the MCFR and DPD coefficients. The added computation brought by the CFR is only the subtraction, which is much less than for CFR methods applied at the DPD input.

Regarding coefficient estimation, the DPD identification is usually based on the input and the output signals of the PA [20]. In [14], the DPD is identified using a closed-loop direct learning architecture (DLA). The model coefficients are estimated iteratively by reducing the error between the PA output and the stimulus. Using indirect learning architecture (ILA),

S. Wang, M. Roger, C. Lelandais-Perrault are with GeePs — Group of electrical engineering - Paris, CNRS, CentraleSupélec, Univ. Paris-Sud, Université Paris-Saclay, Sorbonne Université, 3 & 11 rue Joliot-Curie, Plateau de Moulon 91192 Gif-sur-Yvette CEDEX, France (e-mail of authors: first-name.surname@centralesupelec.fr).

J. Sarrazin is with the Sorbonne Université, Laboratory of Electronics and Electromagnetism, L2E, F-75005 Paris, France (e-mail: julien.sarrazin@upmc.fr).

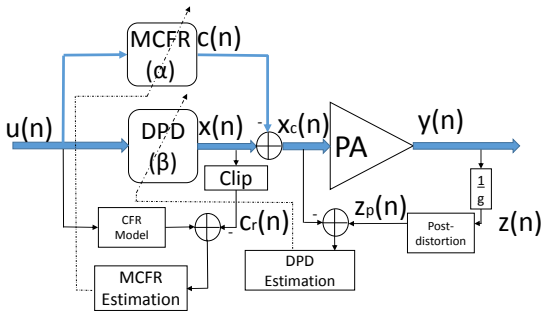

Fig. 1: Joint CFR/DPD general idea

the DPD is identified as a post-distortion block minimizing the error between its output and the PA input when its own input is the PA output.

The CFR model coefficients can be estimated in a similar way using the stimulus and a reference correction signal. The reference correction signal in [14] is generated by clipping the predistorted signal using CAF. However, the CAF applied at the DPD ouput does not reach as good a linearization performance as the CAF applied at the DPD input [18]. In [21], we proposed a clipping-and-bank-filtering (CABF) approach based on a decomposition of the DPD output signal to improve the MCFR applied at the DPD output for single-carrier stimuli. Simulations showed promising results.

This paper generalizes the method to multi-carrier stimuli and demonstrates its validity with experimental results. It also discusses the choice of windows for the CABF decomposition filters and proposes a multiple-step procedure to find the optimal model structure for the joint CFR/DPD. The testbench for validation uses a real PA, first with a single-carrier then a 2-carrier 20 MHz long term evolution (LTE) signal.

This paper is organized as follows. Section II presents the structure of the joint CFR/DPD. The different approaches to compute the reference correction signal for single-carrier and multi-carrier stimuli are detailed in Section III. The proposed multiple-step optimization algorithm is exposed in Section IV. In Section V, the experimental results are presented and discussed. Finally, the conclusion is given in Section VI.

II. Joint CFR/DPD

The joint CFR/DPD general idea is illustrated in Fig. 1. The DPD and the MCFR share the same model structure Φ, respectively with parameters β and α, so that

$$\begin{aligned} c(n) &= \Phi_\alpha[u(n)] \\ x(n) &= \Phi_\beta[u(n)], \end{aligned} \tag{1}$$

where $u(n)$ is the system input signal or stimulus, $c(n)$ the MCFR output and $x(n)$ the DPD output. Thus the clipped predistorted signal $x_c(n)$ is

$$x_c(n) = x(n) - c(n) = \Phi_\theta[u(n)] \tag{2}$$

where $\theta = \beta - \alpha$ represents the vector of the joint CFR/DPD model coefficients.

A. Model Structure

Studies in [22] [23] show that GMP model structure has good linearization performance compared with other mathematical models. Moreover, since it is linear w.r.t. its parameters, the identification can be performed simply with least squares (LS). In this paper, we use GMP for the joint CFR/DPD model structure, which can be written as

$$\begin{aligned} \Phi_\gamma[u(n)] = &\sum_{k=0}^{\mathcal{K}_a-1}\sum_{l=0}^{\mathcal{L}_a-1} \gamma_{a,kl} u(n-l)|u(n-l)|^k \\ &+ \sum_{k=1}^{\mathcal{K}_b}\sum_{l=0}^{\mathcal{L}_b-1}\sum_{m=1}^{\mathcal{M}_b} \gamma_{b,klm} u(n-l)|u(n-l-m)|^k \\ &+ \sum_{k=1}^{\mathcal{K}_c}\sum_{l=0}^{\mathcal{L}_c-1}\sum_{m=1}^{\mathcal{M}_c} \gamma_{c,klm} u(n-l)|u(n-l+m)|^k \end{aligned} \tag{3}$$

where k is the index for nonlinearity, and l, m are the indices for memory. The vector $\gamma = [\gamma_a, \gamma_b, \gamma_c]$ contains the complex coefficients of the signal and envelope, the signal and lagging envelope, and the signal and leading envelope, respectively. $\mathcal{K}_a$, $\mathcal{K}_b$, $\mathcal{K}_c$ are the highest orders of nonlinearity. $\mathcal{L}_a$, $\mathcal{L}_b$, $\mathcal{L}_c$ are the highest memory depths. $\mathcal{M}_b$, $\mathcal{M}_c$ denote the longest lagging and leading delay tap length, respectively.

B. Model Identification

The identification of the joint CFR/DPD in Fig. 1 is based on ILA. We estimate the values of α and β iteratively and alternatingly. The initial value of $\boldsymbol{\alpha}$ is an array of 0. The initial value of $\boldsymbol{\beta}$ is $[1, 0, \cdots, 0]$. Thus at the first iteration, $\boldsymbol{x_c} = \boldsymbol{u}$. We repeat for several iterations until the performance is stable.

A post-distortion block is first identified using the PA input $x_c(n)$ and the signal $z(n)$ which is the PA output $y(n)$ divided by g, the desired loop gain. As different possible choices for g achieve about the same PA efficiency [24], we choose the small signal gain in this paper.

As mentioned above, one advantage of choosing a model structure derived from Volterra series is that the model coefficients can be estimated by solving a linear problem. We can express the post-distortion using matrix notation for a block of N samples:

$$\boldsymbol{z_p} = \mathbf{Z}\boldsymbol{\beta} \tag{4}$$

where $\boldsymbol{z_p} = [z_p(1), \ldots, z_p(N)]^T$, $\boldsymbol{z} = [z(1), \ldots, z(N)]^T$, $\mathbf{Z}$ is $N \times R$ matrix containing basis functions of $\boldsymbol{z}$, and $R = \mathcal{K}_a\mathcal{L}_a + \mathcal{K}_b\mathcal{L}_b\mathcal{M}_b + \mathcal{K}_c\mathcal{L}_c\mathcal{M}_c$ is the total number of coefficients. The LS estimation of $\boldsymbol{\beta}$ is found by

$$\hat{\boldsymbol{\beta}} = [\mathbf{Z}^H\mathbf{Z}]^{-1}\mathbf{Z}^H\boldsymbol{x_c} \tag{5}$$

which minimizes the cost function

$$C = \sum_{n=1}^{N} |z_p(n) - x_c(n)|^2. \tag{6}$$

The identified post-distortion is then applied upstream of the PA as the DPD.

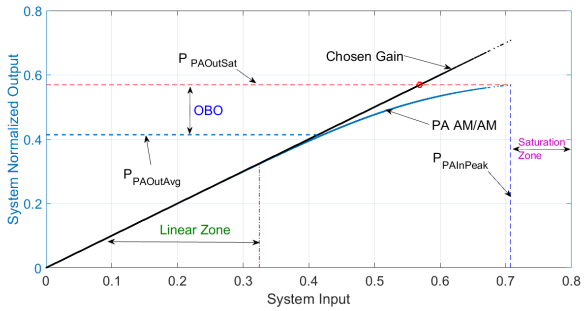

Fig. 2: PA output signal vs PA input signal

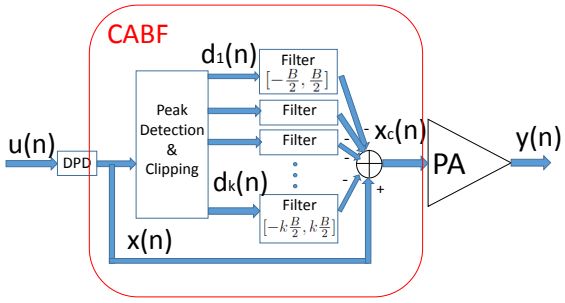

Fig. 3: Validation of CABF

With the current estimate $\hat{\boldsymbol{\beta}}$, the CFR model coefficients can be estimated to reduce the PAPR at the DPD output by

$$\hat{\boldsymbol{\alpha}} = [\mathbf{U}^H\mathbf{U}]^{-1}\mathbf{U}^H\boldsymbol{c_r} \tag{7}$$

where $\boldsymbol{U}$ is the basis function matrix of $\boldsymbol{u}$ and $\boldsymbol{c_r}$ is the vector of reference correction signal.

Since α is estimated according to $\boldsymbol{u}$ and $\boldsymbol{c_r}$, the generation method of $\boldsymbol{c_r}$ has a great impact on the system performance. Simulations previously showed that a CABF approach could outperform the conventional CAF approach in generating $\boldsymbol{c_r}$ [21]. The next section presents an extension of the CABF approach to multi-carrier input signals.

III. Computation of the Reference Correction Signal

The reference correction signal is determined using a clipped version of the DPD output to limit the PA input under a certain threshold. The maximum PA input peak power P_{PAinPeak} is constrained by its corresponding output power being the edge of the PA saturation zone as shown in Fig. 2. In the following, we denote the clipping threshold of the CFR with $P = P_{\text{PAinPeak}}$.

With traditional hard clipping the reference correction signal generated is

$$c_r^{hc}(n) = \begin{cases} x(n)(1 - \frac{P}{|x(n)|}) & \text{if } |x(n)| \geq P, \\ 0 & \text{otherwise,} \end{cases} \tag{8}$$

whereas conventional CAF with ideal rectangular window can be expressed as

$$\mathcal{F}\{c_r^{caf}\} = \begin{cases} \mathcal{F}\{c_r^{hc}\}(\omega) & \text{if } \omega \in [-\frac{B}{2}, \frac{B}{2}], \\ 0 & \text{otherwise,} \end{cases} \tag{9}$$

where B is the bandwidth of the stimulus $u(n)$ and $\mathcal{F}\{\cdot\}$ represents Fourier Transform.

The CABF method is detailed below first for a single-carrier stimulus, then generalized to multi-carrier input signals.

A. Single-Carrier Stimulus CABF

In this section, we consider only the stimulus with one carrier. Noticing that the predistorted signal $x(n)$ contains the nonlinearities of $u(n)$ according to (3) and (1), the bandwidth B is not appropriate for $x(n)$. We decompose $x(n)$ into signals of different nonlinearity orders as

$$x(n) = \sum_{k\in\mathcal{K}} g_k(n) \tag{10}$$

where

$$\begin{aligned} g_k(n) = &\sum_{l=0}^{\mathcal{L}_a-1} \beta_{a,kl} u(n-l)|u(n-l)|^{k-1} \\ &+ \sum_{l=0}^{\mathcal{L}_b-1}\sum_{m=1}^{\mathcal{M}_b} \beta_{b,klm} u(n-l)|u(n-l-m)|^{k-1} \\ &+ \sum_{l=0}^{\mathcal{L}_c-1}\sum_{m=1}^{\mathcal{M}_c} \beta_{c,klm} u(n-l)|u(n-l+m)|^{k-1} \end{aligned} \tag{11}$$

is the term with nonlinearity order k. Since $u(n)$ is limited in $[-\frac{B}{2}, \frac{B}{2}]$, the spectrum of $g_k(n)$ occupies the band $[-k\frac{B}{2}, k\frac{B}{2}]$. In order to keep the nonlinearity information in $x(n)$, we clip and filter each $g_k(n)$ separately within corresponding bands.

First we detect the peaks of $x(n)$ to get the clipped signal $d_k(n)$ corresponding to each $g_k(n)$:

$$d_k(n) = \begin{cases} g_k(n)(1 - \frac{P}{|x(n)|}) & \text{if } |x(n)| \geq P, \\ 0 & \text{otherwise.} \end{cases} \tag{12}$$

Then $d_k(n)$ is filtered in different bandwidth:

$$\mathcal{F}\{d_k^{caf}\} = \begin{cases} \mathcal{F}\{d_k\}(\omega) \cdot W_k(\omega) & \text{if } \omega \in [-k\frac{B}{2}, k\frac{B}{2}], \\ 0 & \text{otherwise} \end{cases} \tag{13}$$

where $W_k(\omega)$ is a window centered at 0 frequency with width $[-k\frac{B}{2}, k\frac{B}{2}]$. Since $g_{k+1}(n)$ occupies a larger band than $g_1(n)$, filtering $d_{k+1}(n)$ increases the errors in bands $[-(k+1)\frac{B}{2}, -\frac{B}{2}]$ and $[\frac{B}{2}, (k+1)\frac{B}{2}]$, which deteriorates the ACPR. Hence we propose to apply windows $W_k(\omega)$ to shape the filters and to smooth out the error.

After repeating the clipping and filtering steps, we apply HC on the final signal to ensure no peak exceeding P. The reference correction signal is finally computed as

$$c_r^{cabf}(n) = x(n) - \sum_{k\in\mathcal{K}} (g_k(n) - d_k^{caf}(n)). \tag{14}$$

The choice of windows $W_k(\omega)$ also has an impact on the linearization performance. We compare different windows by

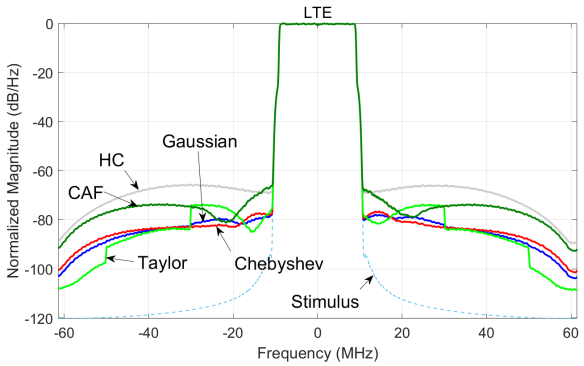

Fig. 4: Test of different windows for CABF

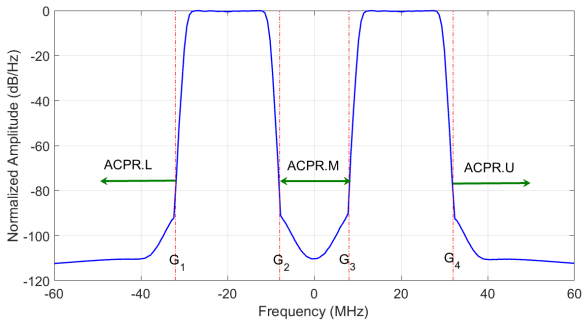

Fig. 5: AMAM & AMPM curves of the PA under test

TABLE I: Impacts on PA linearity with different windows for CABF

Window Name	ACPR (dBc): Front			
	L1	U1	L2	U2
HC	-64.1	-64.0	-65.5	-66.5
CAF	-71.5	-71.1	-72.0	-72.3
Hann	-76.3	-75.2	-83.5	-84.7
Gaussian	-76.7	-75.9	-82.1	-83.0
Hamming	-75.4	-74.4	-82.8	-83.7
Kaiser	-71.3	-71.3	-78.6	-79.0
Blackman	-77.1	-76.2	-82.5	-83.5
Bohman	-77.3	-76.3	-82.4	-83.3
Bartlett	-74.7	-74.0	-81.3	-82.3
Chebyshev	-77.3	-76.6	-81.4	-82.1
Taylor	-74.0	-73.4	-83.2	-83.6

L(U)1(2): First(Second) lower(upper) adjacent channel

passing the clipped signal $s(n) = x(n) - c_r^{cabf}(n)$ to the PA and evaluating the corresponding PA output signals as shown in Fig. 3. A Wiener model PA with saturated output power at 25 dBm is used for the simulation. A 20 MHz LTE signal with 614400 samples is used as stimulus. Its PAPR at the 10^{-4} probability level is 8 dB. The spectra of the PA output are illustrated in Fig. 4. The ACPR values are listed in Table I. The Chebyshev window can reach the best first channel ACPR values (ACPR.L1 and ACPR.U1) and will be used in this paper.

B. Multi-Carrier Stimulus CABF

In the case where the stimulus consists of multiple carriers, the errors in the channels between carriers cannot be reduced with single-carrier CABF since they are regarded as in-band error. Taking the example of a two-carrier signal as Fig. 5, the ACPR needs to be improved not only in lower (ACPR.L) and upper channels (ACPR.U) but also the middle channel (ACPR.M), whose frequency band is $[G_2, G_3]$.

We can reduce the values of ACPR.L and ACPR.U using the method (13) in the previous section. However, in order to filter the middle channels, the windows need to be adapted in the band $[G_2, G_3]$.

In the case of a T-carrier stimulus, we denote B_i the bandwidth of component $x_i(n)$ where $i = 1, \cdots, T$. The band occupied by $x_i(n)$ is $[G_{2i-1}, G_{2i}]$. The filter bank should respect the middle channels $[G_{2i-2}, G_{2i-1}]$ where $i = 2, \cdots, T$.

We create a group of windows $W_k^i(\omega)$ in band $[-k\frac{B_i}{2}, k\frac{B_i}{2}]$ centering at the i-th carrier frequency f_c^i. An inner window is then obtained by combining $W_k^i(\omega)$ into:

$$\Omega_k(\omega) = \max\left(W_k^i(\omega)\right),\ \omega \in [-k\frac{B}{2}, k\frac{B}{2}]. \tag{15}$$

This inner window is only applied on the middle channels:

$$\mathcal{F}\{d_k^{caf}\} = \begin{cases} \mathcal{F}\{d_k\}(\omega) \cdot W_k(\omega) & \text{if } \omega \in \mathcal{O}, \\ \mathcal{F}\{d_k\}(\omega) \cdot \Omega_k(\omega) & \text{if } \omega \in \mathcal{U}, \\ 0 & \text{otherwise} \end{cases} \tag{16}$$

where side channels $\mathcal{O} = [-k\frac{B}{2}, G_1] \cup [G_{2T}, k\frac{B}{2}]$, and middle channels $\mathcal{U} = [G_2, G_3] \cup \ldots \cup [G_{2T-2}, G_{2T-1}]$. The reference correction signal is then obtained by (14).

IV. Model Structure Determination

With the algorithm in [25], we can determine an optimal DPD model structure w.r.t. the trade-off between modeling accuracy and model complexity. The modeling accuracy is represented by (6), which only needs the PA input and output signals to be estimated.

However the model structure for the joint CFR/DPD cannot be determined solely with these signals because it also represents the nonlinearity of the CFR. To find out the optimal model structure, the signal with the best linearization performance after clipping is needed. The difficulty is that the performance of the CABF method depends on the joint CFR/DPD model structure itself.

Considering this, we propose the following multiple-step method to approach the optimal structure:

1) Capture the PA input and output signals to obtain the original structure M_o which is the optimal DPD model.
2) Estimate the coefficients $\boldsymbol{\beta}$ of M_o to linearize the PA and apply the proposed offline CABF on the output signal of M_o.
3) Repeat the second step for several iterations until the performance are stable, similarly to the procedure described in II-B but without estimating the CFR coefficients $\boldsymbol{\alpha}$.
4) Take the stimulus and the CABF output signal (which is the PA input signal) to find a solution structure M_s for the joint CFR/DPD using the algorithm in [25].

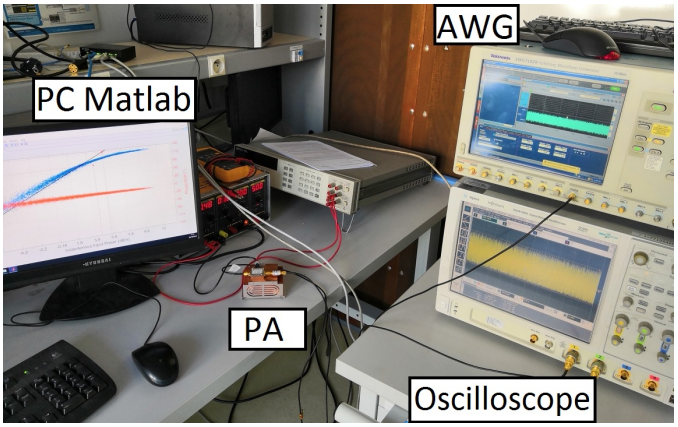

Fig. 6: Test bench for Experimental Implementation

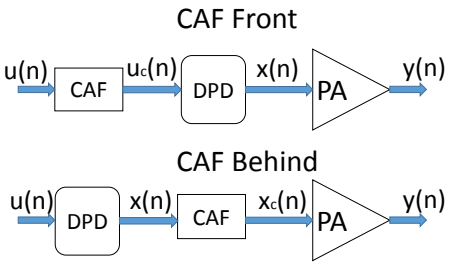

Fig. 7: The structure of CAF in front of and behind DPD

In this algorithm, the CABF output signal at the end of step 3 is considered as the optimal clipped predistorted signal that the joint CFR/DPD output should approach.

This proposed multiple-step method could be iterated substituing M_s as the original structure for the next iteration until the structure is stable. In the following experimental implementations, we use the solution structure without iteration.

V. Experimental results

A. Test bench

The test bench is illustrated in Fig. 6.

The PA in the test bench is a TA020-060-30-27 PA fabricated by Transcom. Its nominal gain is 30 dB and the output power at 1dB gain compression is 27 dBm.

We generate the modulated signal with a carrier frequency of 2 GHz in the PC Workstation and feed it to the PA through an Arbitrary Waveform Generator (AWG) with 10 GHz sampling frequency.

The PA output signal is captured by an oscilloscope and is fed back to the PC workstation for postdistortion processing. The input and output baseband signals are synchronized in time after down-sampling to 120 MHz to be used by the identification algorithm.

B. Joint CFR/DPD model structure

In this section we use as stimulus a 20 MHz LTE signal with a peak-to-average power ratio (PAPR) equal to 8 dB. With the PA input and output signals, the optimal DPD model structure M_o is

$$\begin{aligned} &\mathcal{K}_a = 2, \mathcal{L}_a = 2 \\ &\mathcal{K}_b = 4, \mathcal{L}_b = 1, \mathcal{M}_b = 2 \\ &\mathcal{K}_c = 3, \mathcal{L}_c = 1, \mathcal{M}_c = 2. \end{aligned} \tag{17}$$

Then for the joint CFR/DPD in the case where the PAPR reduction is 1 dB, the optimal structure M_s is

$$\begin{aligned} &\mathcal{K}_a = 6, \mathcal{L}_a = 2 \\ &\mathcal{K}_b = 5, \mathcal{L}_b = 1, \mathcal{M}_b = 2 \\ &\mathcal{K}_c = 3, \mathcal{L}_c = 2, \mathcal{M}_c = 1. \end{aligned} \tag{18}$$

For a PAPR reduction of 2 dB, the model structure is

$$\begin{aligned} &\mathcal{K}_a = 5, \mathcal{L}_a = 3 \\ &\mathcal{K}_b = 2, \mathcal{L}_b = 4, \mathcal{M}_b = 1 \\ &\mathcal{K}_c = 1, \mathcal{L}_c = 4, \mathcal{M}_c = 2. \end{aligned} \tag{19}$$

And when the PAPR reduction is 3 dB, the model structure is

$$\begin{aligned} &\mathcal{K}_a = 5, \mathcal{L}_a = 2 \\ &\mathcal{K}_b = 2, \mathcal{L}_b = 4, \mathcal{M}_b = 1 \\ &\mathcal{K}_c = 1, \mathcal{L}_c = 1, \mathcal{M}_c = 1. \end{aligned} \tag{20}$$

Comparing (17) with (18), we notice that the addition of the CFR asks for a higher nonlinearity order. Furthermore, according to (18) and (19), a greater PAPR reduction requires more memory effects. On the other hand, when the PAPR reduction becomes 3 dB, the number of coefficients is reduced. This can be explained because we optimize the tradeoff between performance and complexity. The greater the PAPR reduction is, the more difficult the linearization becomes. At some point, the performance improvement by the added complexity becomes insufficient to justify a more complex model structure. Therefore the structure (20) keeps the maximum nonlinearity order and memory depth of (19) but decreases the third branch (branch of $\mathcal{K}_c$), which reduces the model complexity without significantly deteriorating the linearization performance.

C. CABF compared to other clipping approaches

In this section we experimentally compare the linearization performance obtained for reference correction signals generated by our Chebyshev-window CABF method to that generated by standard CAF applied on the DPD output. Even though it cannot be used to generate refererence correction signals for MCFR, we also consider CAF applied on the DPD input as a reference since it has the best performance on adjacent channels compared to other CFR methods in [18]. The structures of the CAF Front and the CAF Behind methods are illustrated in Fig. 7.

The obtained PA output spectra are shown in Fig. 8, Fig. 9, and Fig. 10 for 1 dB, 2 dB, and 3 dB PAPR reduction respectively. The corresponding ACPR and EVM values are given in Table II. All approaches keep the EVM below 7%. The DPD without PAPR reduction reaches -45 dBc ACPR at the PA output.

Table II confirms that the CAF in front of the DPD has better linearization performance than the CAF behind the

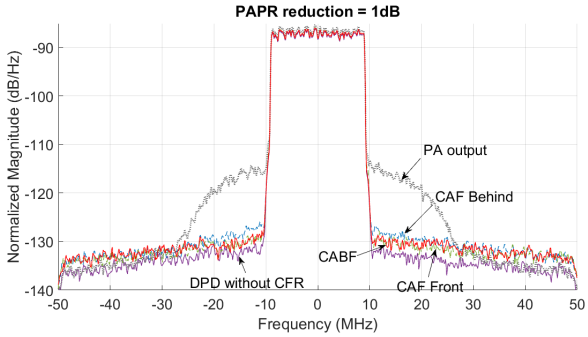

Fig. 8: Linearization performance of different clipping approaches for 1 dB PAPR reduction

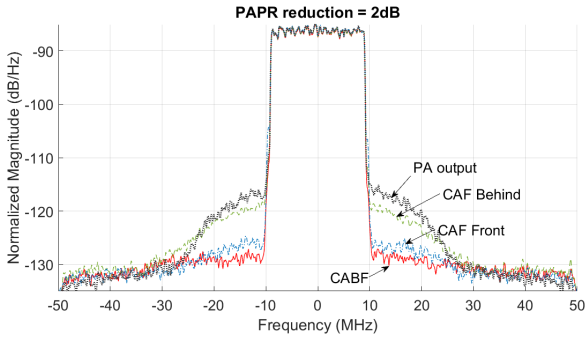

Fig. 9: Linearization performance of different clipping approaches for 2 dB PAPR reduction

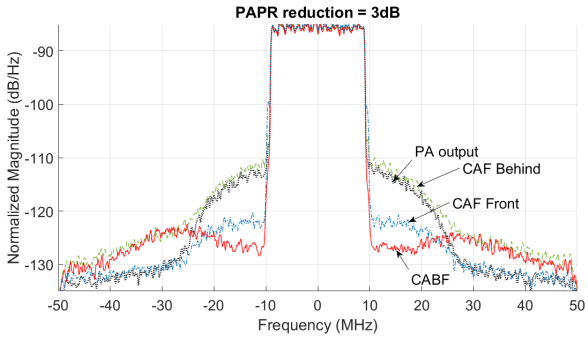

Fig. 10: Linearization performance of different clipping approaches for 3 dB PAPR reduction

TABLE II: ACPR and EVM of different clipping approaches

PAPR gain	CFR Method	ACPR (dBc)				EVM (%)
		L1	U1	L2	U2	
0	DPD without CFR	-44.9	-45.8	-48.9	-48.9	2.55
1 dB	CAF Front	-43.7	-43.7	-46.3	-47.1	2.50
	CAF Behind	-42.3	-42.2	-46.7	-46.1	3.35
	CABF	-43.3	-43.1	-46.2	-46.6	2.48
2 dB	CAF Front	-41.7	-41.7	-46.6	-46.6	2.62
	CAF Behind	-36.1	-36.9	-45.3	-45.5	3.83
	CABF	-42.7	-42.3	-45.8	-46.3	3.37
3 dB	CAF Front	-38.9	-39.0	-47.5	-47.3	3.21
	CAF Behind	-28.6	-28.8	-43.6	-44.0	6.90
	CABF	-38.5	-39.6	-43.6	-44.0	3.98

CAF Front: CAF applied in front of DPD
CAF Behind: CAF applied behind DPD

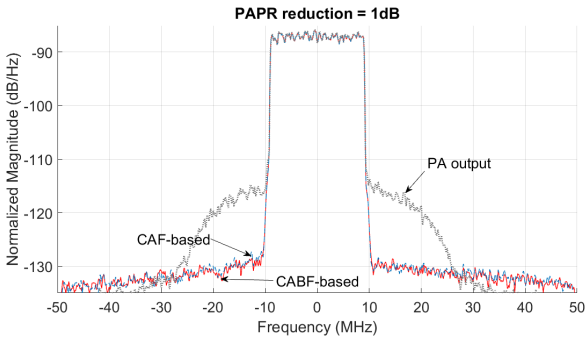

Fig. 11: Test of joint CFR/DPD approaches for 1 dB PAPR reduction

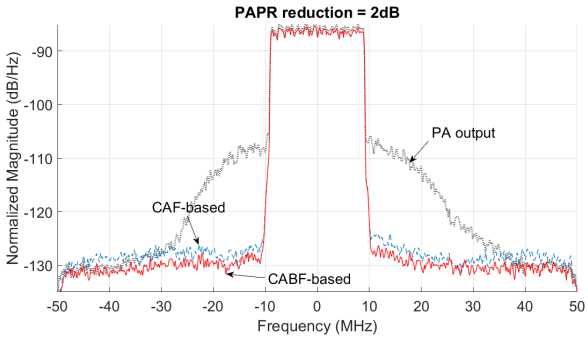

Fig. 12: Test of joint CFR/DPD approaches for 2 dB PAPR reduction

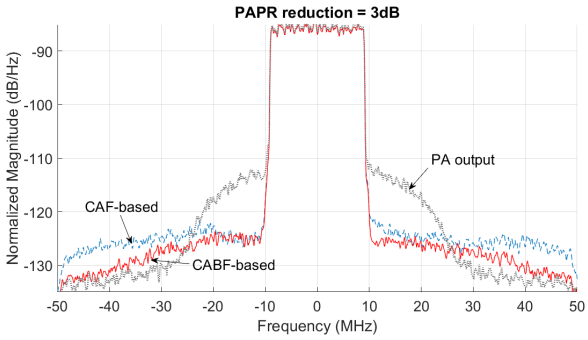

Fig. 13: Test of joint CFR/DPD approaches for 3 dB PAPR reduction

TABLE III: Impacts on PA linearity with joint CFR/DPD

PAPR gain	Joint CFR/DPD	ACPR (dBc)				EVM (%)
		L1	U1	L2	U2	
1 dB	CAF-based	-43.2	-43.1	-46.0	-46.7	2.44
	CABF-based	-43.4	-43.3	-46.3	-46.8	2.43
2 dB	CAF-based	-40.8	-41.0	-42.7	-43.3	2.61
	CABF-based	-42.6	-42.6	-44.0	-43.4	2.52
3 dB	CAF-based	-38.0	-38.5	-40.9	-41.6	3.69
	CABF-based	-39.4	-40.1	-45.2	-45.8	3.73

CAF-based CFR/DPD: Reference correction signal generated by CAF Behind
CABF-based CFR/DPD: Reference correction signal generated by CABF

DPD. However, as said above, it cannot be used for MCFR, which has a huge advantage on the computational complexity [18]. For each value of the PAPR reduction, the CABF can reach the same level of linearization performance as CAF Front and always outperforms the CAF Behind. When the PAPR reduction is 1 dB, the difference of ACPR between CABF and CAF Behind is around only 1 dB. However for greater values, the advantage of CABF becomes more and more important. It reaches 10 dB on the first adjacent channels when the PAPR reduction is 3 dB.

D. CABF-based Joint CFR/DPD

The CABF-based joint CFR/DPD is tested in this section. We use Chebyshev windows for the filtering. There are four iterations for the DPD convergence.

The PA output spectra linearized with different joint CFR/DPD approaches are illustrated in Fig. 11, Fig. 12 and Fig. 13 for 1 dB, 2 dB and 3 dB PAPR reduction respectively. The corresponding ACPR and EVM values are given in Table III. The EVM values of all approaches are less than 4%.

We take the CAF-based joint CFR/DPD model as denoted by "CAF-based" as the reference. When the PAPR reduction is 1 dB, the performance of the CABF-based joint CFR/DPD and the CAF-based joint CFR/DPD is almost the same. When the PAPR reduction is 2 dB and 3 dB, the ACPR values of the CABF-based joint CFR/DPD on the first adjacent channels have an advantage of nearly 2 dB. We also notice that the ACPR differences on the second adjacent channels between these two approaches are almost 5 dB when the PAPR reduction is 3 dB. The PA output spectrum of the CABF-based joint CFR/DPD is also more symmetric in Fig. 13.

To be noticed, the joint CFR/DPD in Table III achieves better linearization performance than the results in Table II. This is because the coefficients of the joint CFR/DPD are estimated iteratively while the DPD coefficients in Section V-C are estimated without the CFR and are fixed during the tests.

These experimental results validate the robustness of the proposed CABF-based joint CFR/DPD. It has good linearization performance though the ACPR values worsen when the PAPR gain increases. The operating point finally depends on the ACPR and EVM requirements. Our proposed method provides larger scale of operating point choice since it gives larger margin on ACPR compared with other approaches.

E. 2-Carrier LTE Stimulus

We test the proposed multi-carrier CABF-based joint CFR/DPD in this section. A 2-carrier LTE signal is used as the stimulus. The lower band carrier frequency is 1960 MHz and the upper band carrier frequency is 2040 MHz. These two components have both 20 MHz bandwidth.

The CFR/DPD model is updated for the 2-carrier stimulus. In the case that PAPR reduction is 1 dB, we use the structure

$$\begin{aligned} &\mathcal{K}_a = 3, \mathcal{L}_a = 1 \\ &\mathcal{K}_b = 2, \mathcal{L}_b = 2, \mathcal{M}_b = 1 \\ &\mathcal{K}_c = 4, \mathcal{L}_c = 4, \mathcal{M}_c = 1. \end{aligned} \tag{21}$$

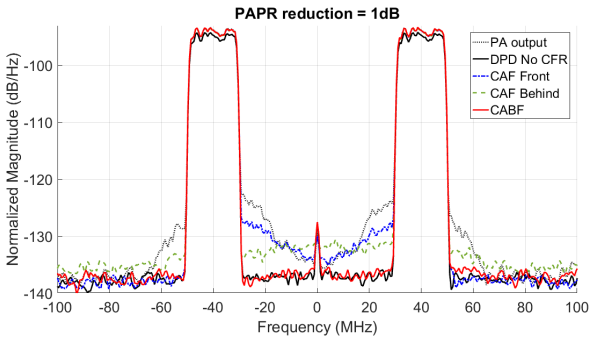

Fig. 14: Linearization performance for 2-carrier stimulus of different CFR approaches for 1 dB PAPR reduction

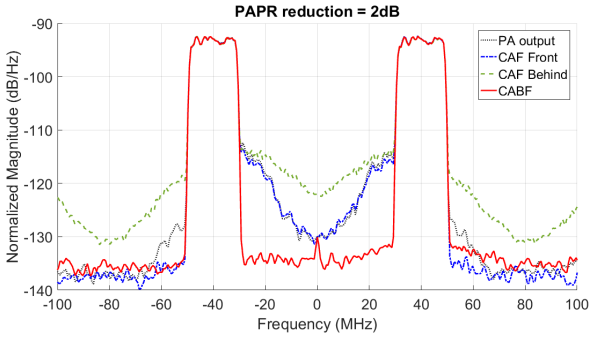

Fig. 15: Linearization performance for 2-carrier stimulus of different CFR approaches for 2 dB PAPR reduction

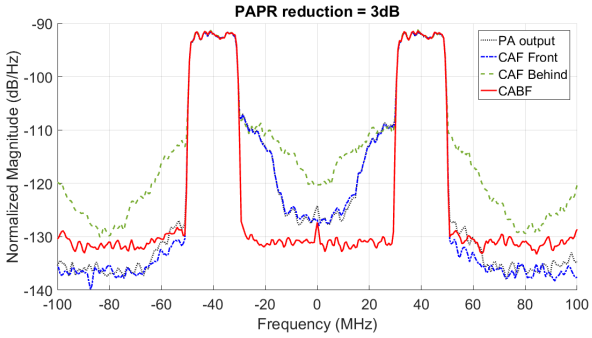

Fig. 16: Linearization performance for 2-carrier stimulus of different CFR approaches for 3 dB PAPR reduction

TABLE IV: ACPR and EVM of different CFR approaches for 2-carrier stimulus

PAPR gain	CFR Method	ACPR.L (dBc)	ACPR.M (dBc)	ACPR.U (dBc)	EVM (%)
0	DPD without CFR	-42.0	-41.0	-41.6	4.18
1 dB	CAF Front	-42.8	-36.3	-42.6	3.55
	CAF Behind	-40.0	-36.7	-39.7	5.28
	CABF	-42.3	-41.6	-41.8	4.57
2 dB	CAF Front	-43.0	-29.4	-42.6	4.67
	CAF Behind	-32.5	-23.6	-32.6	9.07
	CABF	-41.7	-39.8	-40.0	4.89
3 dB	CAF Front	-42.3	-26.5	-42.3	3.61
	CAF Behind	-29.9	-20.9	-29.8	18.97
	CABF	-38.0	-37.9	-37.9	5.21

ACPR.L: ACPR on [-90MHz,-50MHz]
ACPR.M: ACPR on [-30MHz,30MHz]
ACPR.U: ACPR on [50MHz,90MHz]

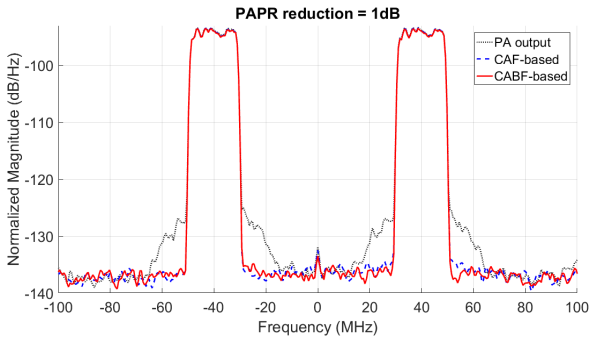

Fig. 17: Test of joint CFR/DPD approaches for 1 dB PAPR reduction

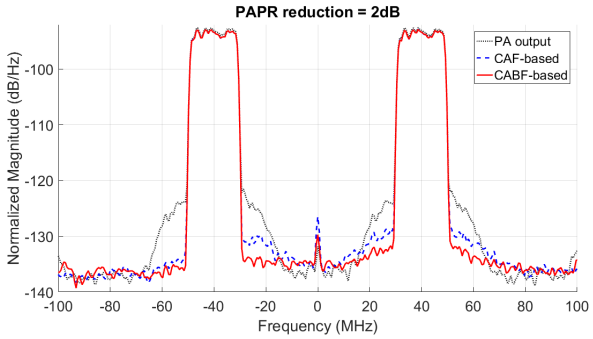

Fig. 18: Test of joint CFR/DPD approaches for 2 dB PAPR reduction

When PAPR reduction are 2 dB and 3 dB, the determined optimal models are MP models with $\mathcal{K}_b = 0$, $\mathcal{K}_c = 0$.

The model structure for 2 dB PAPR reduction is $\mathcal{K}_a = 5$, $\mathcal{L}_a = 3$ and the model structure for 3 dB PAPR reduction is $\mathcal{K}_a = 5$, $\mathcal{L}_a = 2$.

We firstly compare the performance of CAF Front, CAF Behind, and CABF by feeding the clipped signals to the PA. The spectra of the corresponding PA output signals under conditions that PAPR reduction is 1, 2, and 3 dB are illustrated in Fig. 14, Fig. 15, and Fig. 16 respectively. The spectrum "PA output" is the PA output spectrum without the joint CFR/DPD. The ACPR on lower and upper sidebands (ACPR.L/U), and on the middle band (ACPR.M) are given along with the EVM in Table IV.

We can see that the performance of the CABF is always better than that of the CAF Behind. The CAF exhibits good performance on sidebands but it cannot reduce ACPR.M. The proposed CABF reaches good performance on both sidebands and middle band.

The joint CFR/DPD can be identified only with the reference correction signal generated by the CAF Behind or the proposed CABF. We compare the performance of CAF-based and CABF-based joint CFR/DPD under the conditions that the PAPR reduction is 1 dB, 2 dB, and 3 dB in Fig. 17, Fig. 18 and Fig. 19 respectively. The ACPR and EVM values are listed in Table V.

The proposed CABF-based joint CFR/DPD achieves good performance on both the sidebands and the middle band. When the PAPR reduction is 1 dB, its ACPR performance is very close to that of the CAF-based joint CFR/DPD. When the PAPR reduction is over 2 dB, it outperforms the CAF-based joint CFR/DPD in both ACPR and EVM. The measurement results validate our proposed CABF-based joint CFR/DPD for multi-carrier stimulus.

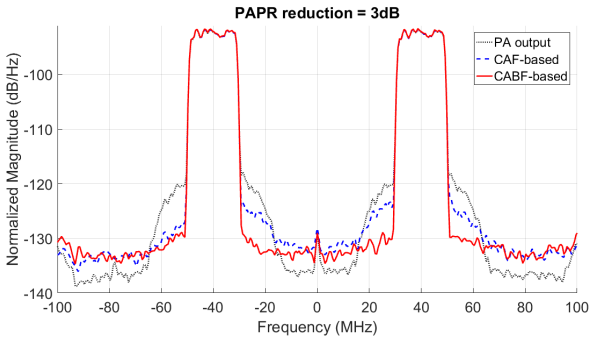

Fig. 19: Test of joint CFR/DPD approaches for 3 dB PAPR reduction

TABLE V: Impacts on PA linearity with joint CFR/DPD

PAPR gain	Joint CFR/DPD	ACPR.L (dBc)	ACPR.M (dBc)	ACPR.U (dBc)	EVM (%)
1 dB	CAF-based	-42.2	-41.1	-41.5	4.13
	CABF-based	-41.8	-41.3	-41.8	6.59
2 dB	CAF-based	-41.8	-38.2	-39.2	4.83
	CABF-based	-41.9	-39.8	-40.6	4.25
3 dB	CAF-based	-38.8	-35.8	-37.2	5.37
	CABF-based	-39.2	-38.8	-38.6	4.92

VI. Conclusion

In this paper, we proposed a CABF-based joint CFR/DPD approach to enhance PA power efficiency while keeping a good linearization performance when the stimulus has one single carrier and multiple carriers. Different types of windows for the CABF are compared. Chebychev windows give the best performance. Experimental results with single-carrier 20 MHz and 2-carrier 20 MHz LTE stimuli validate the proposed approach for various values of PAPR reduction. It reaches linearization performance similar to the much more complex best CFR approaches, e.g. classical CAF in front of DPD. And it outperforms CFR approaches with comparable complexity.

References

[1] L. Guan and A. Zhu, "Green communications: Digital predistortion for wideband rf power amplifiers," *IEEE Microw. Mag.*, vol. 15, no. 7, pp. 84–99, Nov 2014.

[2] F. Raab, "Efficiency of doherty rf power-amplifier systems," *IEEE Trans. Broadcast.*, vol. BC-33, no. 3, pp. 77–83, Sept. 1987.

[3] A. Katz, J. Wood, and D. Chokola, "The evolution of pa linearization: From classic feedforward and feedback through analog and digital predistortion," *IEEE Microw. Mag.*, vol. 17, no. 2, pp. 32–40, Feb 2016.

[4] J. Kim and K. Konstantinou, "Digital predistortion of wideband signals based on power amplifier model with memory," *Electronics Letters*, vol. 37, no. 23, pp. 1417–1418, Nov 2001.

[5] L. Ding, G. Zhou, D. Morgan, Z. Ma, J. Kenney, J. Kim, and C. Giardina, "A robust digital baseband predistorter constructed using memory polynomials," *IEEE Trans. Commun.*, vol. 52, no. 1, pp. 159–165, Jan. 2004.

[6] D. Morgan, Z. Ma, J. Kim, M. Zierdt, and J. Pastalan, "A generalized memory polynomial model for digital predistortion of rf power amplifiers," *IEEE Trans. Signal Process.*, vol. 54, no. 10, pp. 3852–3860, Oct. 2006.

[7] A. Zhu, J. Pedro, and T. Brazil, "Dynamic deviation reduction-based volterra behavioral modeling of rf power amplifiers," *IEEE Trans. Microw. Theory Techn.*, vol. 54, no. 12, pp. 4323–4332, Dec 2006.

[8] F. Mkadem, M. C. Fares, S. Boumaiza, and J. Wood, "Complexity-reduced volterra series model for power amplifier digital predistortion," *Analog Integrated Circuits and Signal Processing*, vol. 79, no. 2, pp. 331–343, 2014.

[9] A. Zhu, "Decomposed vector rotation-based behavioral modeling for digital predistortion lt;newline/ gt;of rf power amplifiers," *IEEE Trans. Microw. Theory Tech.*, vol. 63, no. 2, pp. 737–744, Feb 2015.

[10] T. Liu, S. Boumaiza, and F. Ghannouchi, "Augmented hammerstein predistorter for linearization of broad-band wireless transmitters," *IEEE Trans. Microw. Theory Techn.*, vol. 54, no. 4, pp. 1340–1349, June 2006.

[11] S. Chen, "An efficient predistorter design for compensating nonlinear memory high power amplifiers," *IEEE Trans. Broadcast.*, vol. 57, no. 4, pp. 856 –865, dec. 2011.

[12] S. Wang, M. Abi Hussein, O. Venard, and G. Baudoin, "Optimal sizing of two-stage cascaded sparse memory polynomial model for high power amplifiers linearization," *IEEE Trans. Microw. Theory Tech.*, vol. 66, no. 9, pp. 3958–3965, Sept 2018.

[13] J. Wood, *Behavioral Modeling and Linearization of RF Power Amplifiers:*, ser. Artech House Microwave Library. Artech House, 2014.

[14] R. N. Braithwaite, "A combined approach to digital predistortion and crest factor reduction for the linearization of an rf power amplifier," *IEEE Trans. Microw. Theory Techn.*, vol. 61, no. 1, pp. 291–302, Jan 2013.

[15] A. Mbaye, G. Baudoin, A. Gouba, Y. Louet, and M. Villegas, "Combining crest factor reduction and digital predistortion with automatic determination of the necessary crest factor reduction gain," in *2014 44th European Microwave Conference*, Oct 2014, pp. 837–840.

[16] X. Chen, W. Chen, F. Huang, F. M. Ghannouchi, Z. Feng, and Y. Liu, "Systematic crest factor reduction and efficiency enhancement of dual-band power amplifier based transmitters," *IEEE Trans. Broadcast.*, vol. 63, no. 1, pp. 111–122, March 2017.

[17] H. Enzinger, K. Freiberger, and C. Vogel, "Competitive linearity for envelope tracking: Dual-band crest factor reduction and 2d-vector-switched digital predistortion," *IEEE Microw. Mag.*, vol. 19, no. 1, pp. 69–77, Jan 2018.

[18] S. Wang, M. Roger, and C. Lelandais-Perrault, "Impacts of crest factor reduction and digital predistortion on linearity and power efficiency of power amplifiers," *IEEE Trans. Circuits Syst. II, Exp. Briefs*, pp. 1–1, 2018.

[19] M. V. Amiri, M. Helaoui, N. Boulejfen, and F. M. Ghannouchi, "Optimized spectrum constrained crest factor reduction technique using polynomials," *IEEE Trans. Commun.*, vol. 63, no. 7, pp. 2555–2564, July 2015.

[20] M. Abi Hussein, V. Bohara, and O. Venard, "On the system level convergence of ila and dla for digital predistortion," in *Wireless Communication Systems (ISWCS), 2012 International Symposium on*, Aug 2012, pp. 870–874.

[21] S. Wang, M. Roger, and C. Lelandais-Perrault, "Clipping-and-bank-filtering technique in joint crest factor reduction and digital predistortion for power amplifiers," in *2018 Asia-Pacific Microwave Conference (APMC)*, Nov 2018, pp. 768–770.

[22] A. S. Tehrani, H. Cao, S. Afsardoost, T. Eriksson, M. Isaksson, and C. Fager, "A comparative analysis of the complexity/accuracy tradeoff in power amplifier behavioral models," *IEEE Trans. Microw. Theory Techn.*, vol. 58, no. 6, pp. 1510–1520, June 2010.

[23] C. Kantana, O. Venard, and G. Baudoin, "Comparison of gmp and dvr models," in *2018 International Workshop on Integrated Nonlinear Microwave and Millimetre-wave Circuits (INMMIC)*, July 2018, pp. 1–3.

[24] S. Wang, M. Abi Hussein, O. Venard, and G. Baudoin, "Impact of the normalization gain of digital predistortion on linearization performance and power added efficiency of the linearized power amplifier," in *2017 12th European Microwave Integrated Circuits Conference (EuMIC)*, Oct 2017, pp. 310–313.

[25] ——, "A novel algorithm for determining the structure of digital predistortion models," *IEEE Trans. Veh. Technol*, vol. 67, no. 8, pp. 7326–7340, Aug 2018.

Siqi Wang received the B.S. degree from Huazhong University of Science and Technology, Wuhan, China in 2012, the M.S. degree from the University of Paris-Sud, Orsay, France in 2014, and the Ph.D. degree from the University of Paris-Est Marne La Vallée, Champs sur Marne, France, in 2018. He is currently a post-doc fellow with GeePs, Centrale-supélec. His research interests include wireless communications, digital predistortion, energy efficiency optimization for wireless communication systems.

Morgan Roger graduated from the Ecole Spéciale des Travaux Publics in Paris in 2002, with an emphasis on mechanics, electrical engineering and electronics. The same year, he joined the Department of Electronic Systems of CentraleSupélec in Gif-sur-Yvette to pursue his Ph.D. in signal processing. He received it from the Paris-Sud University (Orsay) in 2007 and is now an associate professor of CentraleSupélec, affiliated with the GeePs laboratory. His current research interests include data converters and signal processing methods for electronic systems with an emphasis on power amplifier linearization.

Caroline Lelandais-Perrault received in 1995 the diploma from the Ecole Supérieure d?Electricité (Supélec), one of the French Grandes Ecoles. She worked six years as a development engineer and project manager at IN-SNEC (Zodiac Data Systems), a company specialized in telemetry equipments for satellites and Ariane rocket. In 2001, she joined the Electronic System Department at Supélec and received her PhD in 2006 from Université Paris XI. She is currently Associate Professor in the Dep. of Electronic Systems of CentraleSupélec at Université Paris-Saclay. With GeePs lab. (UMR CNRS 8507), her research activities concern wide-band and versatile and also high resolution analog-to-digital conversion and focus especially on calibration techniques of that systems.

Julien Sarrazin received his Engineering diploma/Master of Research, and PhD degrees from the University of Nantes in France, in 2005 and 2008 respectively. In 2009 and 2010, he worked at the BK Birla Institute of Technology of Pilani, in India, where he was in charge of telecommunication-related teaching. In 2011 and 2012, he was a research engineer at Telecom ParisTech in Paris. Since September 2012, he is an Associate Professor at Sorbonne Université (formerly University of Pierre and Marie Curie) in Paris, where he is currently working in the Electronics and Electromagnetism Lab (L2E) in the field of Spatial Data Focusing and localization. His research interests also include antenna design, channel modeling for Body Area Networks. He is an IEEE member and reviewer and has published over 90 technical journals, patents, book chapters, and conference papers.